# Water Dynamics in Graphite Oxide Investigated with Neutron Scattering

**Alexandra Buchsteiner,*,† Anton Lerf,‡ and Jörg Pieper§**

*Hahn-Meitner-Institut, Glienicker Strasse 100, D-14109 Berlin, Germany, Walther-Meissner-Institut der Bayerischen Akademie der Wissenschaften, D-85748 Garching, Germany, and Technical University Berlin, D-10623 Berlin, Germany*

*Received: June 30, 2006; In Final Form: September 1, 2006*

Graphite oxide is an inorganic multilayer system that preserves the layered structure of graphite but not the conjugated bond structure. In the past few years, detailed studies of the static structure of graphite oxide were carried out. This was mainly done by NMR investigations and led to a new structural model of graphite oxide. The layer distance of graphite oxide increases with increasing humidity level, giving rise to different spacings of the carbon layers in the range from 6 to 12 Å. As a consequence, different types of motions of water and functional groups appear. Information about the mobility of the water molecules is not yet complete but is crucial for the understanding of the structure of the carbon layers as well as the intercalation process. In this paper, the hydration- and temperature-dependent dynamic behavior of graphite oxide will be investigated by quasielastic neutron scattering using the time-of-flight spectrometer NEAT at the Hahn-Meitner-Institut Berlin. The character of the embedded water does not change over a wide range of hydration levels. Especially the interlayer water remains tightly bound and does not show any translational motion. In samples with excess water, however, the water is also distributed in noninterlayer voids, leading to the observation of additional motions of bulklike or confined water. The dynamic behavior of hydrated graphite oxide can be described by a consistent model that combines two two-site jump motions for the motions of the water molecules and the motions of OH groups.

## 1. Introduction

Graphite oxide (GO) has been known and used since the 19th century.[1] Recent interest grew from a proposed application as material for battery electrodes[2−4] membrane models,[5−7] because of the possibility of intercalation and for the formation of artificial layered nanocomposites containing proteins and synthetic polymers by the layer by layer deposition method.[8,9]

Graphite oxide is a nonstoichiometric compound. The lower and upper limits of the C:O:H ratio are 6:2.33:1.2 and 6:3.7:2.83, respectively.[10−18] Depending on the conditions of oxidation during the preparation process, GO may contain variable amounts of oxygen. The lowest carbon contents, i.e., the highest oxygen contents, are normally encountered in the samples prepared by the Staudenmeier method,[19] the lowest one for the Brodie method.[1] However, there is also a big scatter within one preparation method, which is due to different particle size, variation in reaction times, and processing details.

Because of the turbostratic stacking of the graphite oxide layers diffraction methods were of very restricted help in determining the structure. Thus, at least five different structure models have been presented over the last 70 years on the basis of chemical arguments, X-ray diffraction, and spectroscopic investigations.[11,12,16,17,20,21] Because of $^{13}$C-NMR measurements[22−26] of the last 15 years, evidence is growing in favor of a structure in which part of the graphite double bonds are broken and replaced by covalently attached OH and epoxide groups; this is a structure very similar to the earlier suggestions of Hofmann and Ruess.[12−14,20]

The most important feature of graphite oxide is its hydrophilic nature, which leads to a complete swelling of the solid and the formation of a colloidal solution in water of very low electrolyte concentration and under slightly basic conditions. Under higher electrolyte concentration and in slightly acidic conditions, the hydration is strongly restricted and the maximum layer distance observed amounts to about 12 Å.

If hydrated graphite oxide is equilibrated in atmospheres of different relative humidities, the layer spacing increases continuously with increasing humidity from about 6 to about 8.6 Å at a relative humidity of 75%.[27,28] This corresponds roughly to the uptake of a water monolayer in the interlayer space of graphite oxide. The layer distance of 12 Å is reached only at even higher humidity after long equilibration times. The resulting layer distances are not defined only by the relative humidity but also by the samples used and the equilibration time.[28] As a consequence of the various layer spacings, different motions of water molecules and functional groups can be expected.

Whereas the hydration behavior is well-documented, nearly no information is available about the mobility of the water molecules, but it is crucial for the understanding of the strong hydrophilicity of GO as well as the intercalation processes.

To get information about the dynamics in hydrated GO, we investigated graphite oxide equilibrated at several humidity levels using quasielastic neutron scattering at NEAT at the Hahn-Meitner-Institut Berlin. We used two different resolutions (35 and 93 $\mu$eV) to cover a broad range of time scales for detecting possible motions. The studies were done with a dependence on humidity and temperature, which provides the possibility of

* Corresponding author. E-mail: buchsteiner@hmi.de. Phone: 49 (0)30 8062-3179. Fax: 49 (0)30 8062-3094.

† Hahn-Meitner-Institut.

‡ Walther-Meissner-Institut der Bayerischen Akademie der Wissenschaften.

§ Technical University Berlin.

10.1021/jp0641132 CCC: $33.50 
Published on Web 10/13/2006

determining the type of motions and assigning these certain motions to moving entities.

Throughout this paper, we will refer to different kinds of water, which should be defined as follows: "bulk water" behaves like normal water without any constraints such as confinement; "confined water" encounters arbitrary constraints coming, for instance, from the vicinity of surfaces but has enough water molecules around so that translational diffusion can take place even if slowed; and "bound water" is relatively tightly bound to its position, allowing only localized motions. The term "excess water" shall cover bulklike as well as confined water.

## 2. Experimental Methods

**2.1. Sample Preparation.** Graphite oxide is prepared by treating graphite with oxidizing agents such as $KClO_3$, $NaClO_3$, or $KMnO_4$ in highly concentrated sulfuric acid, nitric acid, or mixtures of both.

There are mainly three different preparation methods that result in samples with different oxygen content and, following from this, different minimal layer distances: Brodie[1] (carbon content 62 wt %, layer distance 5.5−5.9 Å), Staudenmaier[19] (52 wt %, 6.3−6.5 Å) and Hummers/Offeman[29] (57 wt %, 6.7−6.9 Å). The properties of the resulting samples[17] depend on the nature of the starting material, details of the preparation procedure, and number of oxidizing cycles.

The samples used for the hydration and neutron scattering investigations presented here were produced by a slightly modified version of Brodie's method.[18,30]

**2.2. Hydration Procedure.** For the time-of-flight neutron scattering measurements, samples with different hydration levels were used.

To get a very homogeneous water distribution, we first saturated the samples with water and afterward dried them to the according hydration level by storing them in humid environments generated by saturated salt solutions, i.e., the samples exchange hydration water with the gas phase above the salt solution until an equilibrium state is reached. The used salts were NaCl for 75% relative humidity (r.h.) and $K_2CO_3$ for 44% relative humidity. To get the highest hydration level, we utilized pure water, causing a relative humidity of 100%. We used Millipore water, as the resulting relative humidities depend strongly on the purity of the salt solutions. The necessary equilibration times ranged from a few days up to several weeks.[28] The amount of the incorporated water was determined for all samples by measurements of the sample weight before and after the hydration process.

In the beginning of our experiments, the change of the layer distance for different humidities was investigated. The resulting layer distances were measured in two ways. Small separate amounts of samples were hydrated independently and the layer distance was measured by X-ray scattering using Ni-filtered Cu-$K_\alpha$ radiation (Bruker AXS, D8 Advance diffractometer). This investigation also gave us the necessary equilibration time for the samples. Additionally, the layer distances could be determined by calculation from the Bragg peaks showing up in the angular spectrum of the time-of-flight spectrometer.

During the preparation of the samples for these studies, we found that the degree of hydration and the kinetics of water uptake depend crucially on the preparation and aging conditions.

**2.3. Quasielastic Neutron Scattering.** The quasielastic neutron scattering measurements were done at the time-of-flight spectrometer NEAT at the Hahn-Meitner-Institut in Berlin.[31]

The powdered samples with different amounts of water were enclosed in slab-shaped aluminum sample containers with a diameter of 50 mm and a thickness of 0.8 mm. The sample orientation was 45° with respect to the incoming beam.

We used experimental resolutions (full width at half maximum) of 93 $\mu$eV ($\lambda = 5.1$ Å, Q range = 0.3−2.3 Å$^{-1}$) and 35 $\mu$eV ($\lambda = 8.0$ Å, Q range = 0.2−1.5 Å$^{-1}$), respectively. The 35 $\mu$eV measurements should enable us to check for slow translational motions that possibly could not be seen with a resolution of 93 $\mu$eV.

The data were corrected for the contribution of the empty container and the different detector efficiencies. A standard vanadium slab of 1 mm thickness was measured to determine the experimental resolution function, which is an almost-perfect Gaussian function for NEAT at reasonable resolution values. For the data analysis, the resolution function was analytically convoluted with the theoretical model scattering function, giving higher accuracy than for numerical convolution.

For all the corrections, standard routines included in the program package FITMO[32] from NEAT were used. To increase the statistics, we grouped the data in 10 angular groups before the transformation to the energy scale.

Because of large transmission values of $T > 0.9$, except for the sample with the highest $H_2O$ content, it was not necessary to correct for multiple scattering.

The temperature was varied in the range between 220 and 320 K, with an accuracy of 0.1 K.

## 3. Results and Discussion

**3.1. Structure of Graphite Oxide.** To describe the water dynamics, we need a reasonable model for the distribution of the functional groups on the carbon network.

The chemical analysis and the appearance of double bonds in the NMR spectra show that the limiting composition expected for full oxidation, i.e. $C_6O_3$, is never reached in any of the graphite oxide samples investigated. Considering the three different functional groups established by the NMR results, the simplest model one can create is based on the assumption that one double bond is unaffected by oxidation, the other double bond is replaced by the epoxide oxygen, and the third one is broken and replaced by two OH functions. Thus, one would end with a tentative composition $C_6O(OH)_2$, which is almost in the range of experimentally determined compositions.

To find a reasonable distribution of functional groups based on this idealized formula, one has to take into consideration the size ratio of carbon and oxygen atoms/ions. Consequently, *cis*-OH groups can be ruled out completely, because the OH functions have to be in upright positions because of the connectivity of the carbons in the graphite layers. Thus, they cannot avoid each other by rotating the carbon frame as in monosaccharide compounds. Even OH functions in meta positions (nomenclature in aromatic six-ring compounds) would be too close together, because the distance of 1,3-carbon atoms is shorter than twice the radius of oxygen atoms/ions. However, the oxygen packing density is naturally reduced through the fact that they are located on both sides of the carbon layers. If one considers a six-ring entity of the graphite sheet and assumes two epoxide functions, both could look upside down. If one of these epoxide groups is replaced by two OH functions, two different arrangements are possible: In the first one, the epoxide function and one of the OH functions are on the same side of the carbon ring and the second OH function is on the other side; this is the case regardless of the starting situation, i.e., whether the two epoxide functions were on the same side of

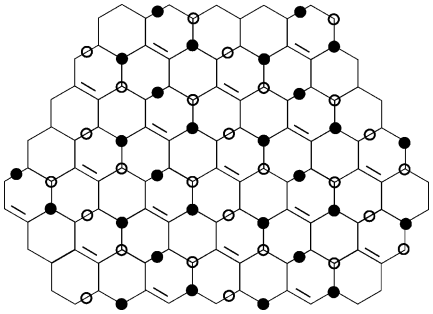

**Figure 1.** Structure of graphite oxide: The graphite oxide layers are mainly flat with OH groups and epoxide groups attached to them. The oxygen atoms of the epoxide groups form layers of variable concentration. The circles mark the positions of OH groups (corners of hexagons) and the position of epoxide groups (edges of hexagons). The filled (hollow) circles indicate groups that are situated above (below) the carbon layer.

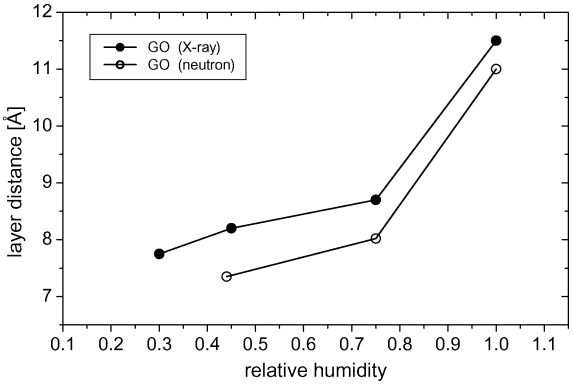


**Figure 2.** Layer distance vs relative humidity, measured with X-ray scattering (solid symbols) and TOF scattering (open symbols). Equilibration times: 21 days for neutron data, 4 days for X-ray data.

the ring or on opposite sides. The other possibility would be that the epoxide function is on one side of the ring and both OH functions are on the opposite side, but in the para position. The question arises how regular these arrangements are distributed on both sides of the carbon grid.

This model can be now used to calculate jump distances for protons. Just one possible distribution (a strongly regular one) is shown in Figure 1. This scheme is a more precise version of our previous model,[24] taking into account the chemical composition of graphite oxide and the geometrical constraints discussed above.

**3.2. Hydration Behavior.** The hydration behavior of the samples was analyzed before the investigation of the dynamics in order to characterize the sample properties and determine the reliability of the hydration process.

Figure 2 shows the resulting relative-humidity-dependent layer distances of one of our investigated samples measured with both X-ray and neutron scattering. The resulting layer distances are not only defined by the relative humidity and the preparation method but also by the equilibration time, i.e., the different preparation methods yield different necessary equilibration times.

The comparison of layer distances measured with X-ray scattering and neutron time-of-flight scattering reveals some deviations. Although the humidity-dependent behavior appears to be consistent for both measurement techniques, the absolute values differ a little bit. These differences could be mainly caused by the different physical entities imaged by the two techniques (electron densities versus scattering lengths of atomic nuclei) and the possible interstratification effect that influences the result to a different extent for both techniques.

During the tests with the preparation and especially the hydration, it turned out that the preparation and equilibration conditions very strongly influence the resulting layer distances and water distributions.

The amount and distribution of oxygen in the graphite oxide sample mainly determines the water uptake properties. The more oxygen present, the more water that can be taken up and the higher the dry layer thickness will be.

Because of the preparation process, a random interstratification of fully (or partly) oxidized and nonoxidized layers seems to be possible. This assumption is supported by the different layer spacings and water uptake properties encountered for samples from different preparation methods.[28] As a consequence, differently oxidized layers can take up different amounts of water during the hydration process. Also, completely empty interlayer spaces could be present. Hence, the hydrated samples end up with interlayer spaces filled with (different amounts of) water and empty interlayer spaces.

Additionally, samples hydrated with $D_2O$ were prepared. With the results from these data, it should have been possible to separate the scattering contributions that stem from the graphite oxide membranes and the water molecules, respectively, because of the very different incoherent scattering cross sections of deuterium and hydrogen. Nevertheless, despite very identical preparation and hydration conditions, during the measurements of layer distances, it turned out that it was not possible to produce $D_2O$-hydrated samples with exactly the same layer distances as $H_2O$-hydrated graphite oxide, thus making a simple separation by subtracting the contributions impossible. The experimentally detected layer distances of $D_2O$ hydrated samples were always lower than those for $H_2O$ hydrated samples. The differences were even higher for the higher hydration levels. In combination with the above-mentioned fact that the resulting layer distances are very sensitive to preparation and hydration conditions, it could be concluded that mainly the different physical properties of $D_2O$ compared to $H_2O$ (lower solubility, lower reactivity, stronger bonding of $D_2O$) caused these differences. Furthermore, a possible H/D exchange in the graphite oxide itself could not be excluded, which may be another reason for the difference of the layer distances.

More detailed data about the hydration process can be found in ref 28.

In the following, we refer to the layer distance of the samples, as this quantity should mainly determine the dynamic behavior of the sample. Furthermore, the layer distance is the more exact value compared with the relative humidity used for the hydration of the samples. It was determined during each time-of-flight measurement, giving actual information about the measured sample.

**3.3. Quasielastic Neutron Scattering.** The dynamic properties of the material were investigated by time-of-flight neutron scattering. We restrict ourselves to the discussion of incoherent scattering, as hydrogen atoms scatter mainly incoherently, and we can neglect the small coherent contributions. The incoherent double-differential cross section

$$\frac{\delta^2\sigma}{\delta\Omega\delta\omega} = \frac{1}{4\pi}\frac{\vec{k}_f}{\vec{k}_i}[b_{inc}^2 S_{inc}(\vec{Q},\omega)] \qquad (1)$$

describes the number of neutrons scattered into a certain angle element $\delta\Omega$ and energy-transfer element $\delta\omega$, where $\vec{k}_i$ and $\vec{k}_f$ are the wave vectors of the incident and scattered neutrons,

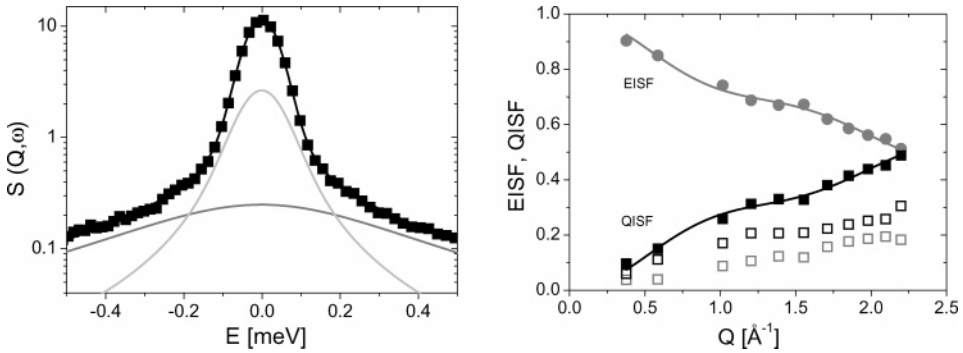


**Figure 3.** Scattering function fitted with phenomenological model (left) and resulting EISF, QISF at $Q = 2.3$ Å$^{-1}$ (right) of a GO sample with 75% r.h. The solid markers in the right picture show the EISF and summed QISF, whereas the hollow markers show the single QISFs for each motion.

respectively, $\vec{Q}$ is the momentum transfer, and $b_{inc}$ is the incoherent scattering length. Using the Van Hove formalism,[33] the incoherent scattering function gives information about the dynamics of (hydrogen) atoms. We analyze the dynamics using the general theoretical incoherent scattering function[34]

$$S(Q,\omega) = e^{-(\hbar\omega/2kT)}\, e^{-\langle u^2\rangle Q^2}[A_0(Q)\delta(\omega) + \sum_n A_n(Q)L_n(\Gamma_n,\omega)] \quad (2)$$

(we use the formula in isotropic approximation without taking into account special motions of certain atoms).

The scattered intensity $S(Q,\omega)$ is separated into an elastic $\delta$-shaped component and a number of quasielastic Lorentzian-shaped contributions parametrized by the width $\Gamma_n = 1/\tau_n$ and the quasielastic incoherent structure factors $A_n$ (QISF). The amplitude of the elastic component is given by the elastic incoherent structure factor (EISF) $A_0$. The Debye-Waller factor $e^{-\langle u^2\rangle Q^2}$ describes the vibrational contributions, where $\langle u^2\rangle$ gives the global averaged mean square displacement (MSD) of the vibrational motions.

The theoretical scattering function $S_{theo}(Q,\omega)$ has to be convoluted with the resolution function $S_{resol}(Q,\omega)$ to get a function that can be used for fitting the measured scattering data

$$S_{measured}(Q,\omega) = Fe^{-(\hbar\omega/2kT)}[S_{theo}(Q,\omega)\otimes S_{resol}(Q,\omega)] \quad (3)$$

where $e^{-(\hbar\omega/2kT)}$ is the detailed balance factor and $F$ is a normalization factor.

In graphite oxide, we expect possible motions of confined or bound water molecules (jumps between certain places, rotational motions) of functional OH groups and bulk water molecules. All of them can be described phenomenologically by a sum of Lorentzian contributions and an elastic contribution as given above.

Starting from the results obtained when using this phenomenological model, we evaluated a physical model that takes into account the structure of the graphite oxide as investigated so far and thus the possible motions in the material. The next section will describe the procedure in more detail.

**3.4. Jump Model.** The motions of protons in hydrated graphite oxide have been investigated in dependence on the humidity level and on temperature. To describe the dynamic behavior, we had to find a model suitable for describing the experimental scattering function.

A first analysis and fit of the data with the purely phenomenological model with a number of Lorentzian functions revealed that we have at least two different quasielastic contributions for small and medium humidities. The half-widths of these Lorentzians appeared to vary very little around a fixed value with $Q$ and were therefore kept constant during the following fits. The correlated motions are thus localized ones.

For very high humidities, a third strong contribution with a strong Q-dependence was encountered, probably describing some kind of long-range diffusion.

Figure 3 (left) shows as an example the result of the fitting procedure (phenomenological model) at $Q = 2.3$ Å$^{-1}$ for a GO sample with 75% r.h. and a layer distance of 8.0 Å. The experimental data were fitted very well, which can be seen very clearly because of the logarithmic scaling of the ordinate. The right picture shows the resulting EISF and QISF values.

According to the proposed graphite oxide structure (see Figure 1), there are two different types of protons that can be engaged in the dynamics of GO: the protons of the water molecules and the protons of the OH groups. The protons of the water molecules can interact with the oxygen atoms of the OH groups, the epoxide oxygens, and the oxygens of neighboring water molecules. The protons of the OH functions can interact with the epoxide oxygens, the oxygens of next-nearest OH functions, and again with the oxygens of water molecules. These interactions may lead to at least two different types of molecular motions: the more or less restricted rotation of water molecules and the motions due to the interaction of the protons of OH functions with other oxygen atoms. In all of these motions, the hydrogen atoms should be able to couple via hydrogen bonds or electrostatic interactions to the nearby oxygens.

As no contributions could be described with the isotropic rotational diffusion model,[34] we expect the discovered localized motions to be two different jump motions with different jump distances and time scales. The types of these jump motions (number of possible jump places, symmetry of jump axis, etc.) are mainly determined by the distribution of the functional groups on the carbon network (see Figure 1).

From this distribution, we conclude that only two- or three-site jumps should be possible. As the epoxide and OH groups are relatively sparsely distributed (at most two per aromatic ring on the same side of the GO layer), we restrict our model to two-site jumps; possible three-site jumps should be too rare to be taken into account. The two sites should be (almost) equivalent places (epoxide groups, oxygens of OH groups). Thus, we use the "two-site jump model between equivalent places" as described in ref 34 for a powdered sample

$$S(Q,\omega) = A_0(Q)\delta(\omega) + A_1(Q)\frac{1}{\pi}\frac{2\tau}{4+\omega^2\tau^2} \quad (4)$$

with

$$A_0(Q) = \frac{1}{2}[1 + j_0(Qd)]$$

$$A_1(Q) = \frac{1}{2}[1 - j_0(Qd)]$$

where $j_0(x)$ is the Bessel function of order zero, $\tau$ is the mean residence time, and $d$ is the jump distance between the two sites. The jump rate is then defined by $r = 1/\tau$. The scattering function has to be averaged over all possible orientations of $Q$.

As we found two quasielastic contributions, we use a double two-site jump model, where each jump motion is weighted by its proportion of the total number of jumps ($g_{1,2}$), where the ratios $g_{1,2}$ work as fit parameters

$$S_{\text{total}}(Q,\omega) = g_1 S_{\text{jump1}}(Q,\omega) + g_2 S_{\text{jump2}}(Q,\omega) \qquad (5)$$

$$g_{1,2} = \frac{\text{number of jump1 or jump2}}{\text{total number of jumps}}$$

At small and medium relative humidities, we did not find any indication for a translational motion of the interlayer water (see Section 3.5), which also supports our hypothesis of the presence of only two localized motions.

In the recent literature, another model, the "relaxing cage model", was favored to describe confined water,[35] with quite good results. It supposes that each water molecule is surrounded by so many neighboring water molecules that they can interact with each other, causing some constraints to the mobility of the water molecules. A basic result is that one can compare the behavior of confined water with that of bulk water at a reduced temperature.

However, this model is not suitable for being applied to our system of hydrated graphite oxide because of very different local environments. In contradiction to that model, we assume to have widely separated water molecules interacting with the OH groups rather than with other water molecules as long as there is no excess water present in the system. We will confirm this assumption in Section 3.8. Thus, the "relaxing cage model" is not appropriate for our membrane system.

To describe the samples with high water content (i.e., samples that contain not only interlayer water but also excess water), we use an additional contribution to describe the excess water. As it should behave as bulklike or confined water, we use the Teixeira model,[36] which consists of a translational jump diffusion and an isotropical rotational diffusion with Sear's expansion.[37] The jump motions and the motions of the excess water were completely separately treated, and the amounts of the single contributions were weighted with the mass ratios.

All experimental data could be fitted with the above-described jump model (plus additional excess water contribution where necessary). Figure 4 shows an example of an experimental data set measured with $\Delta E = 93\ \mu$eV, the fitted scattering function, and the single quasielastic contributions.

The calculated jump distances were 3.05 Å (referred to as "long jumps", i.e., "jump 1") and 1.46 Å ("short jumps", i.e., "jump 2") at 296 K. We will discuss the assignment of the jump motions to certain flexible entities in Section 3.6.

In the following, the double two-site jump model with possible excess water contribution established in this section will be used exclusively.

**3.5. Scattering Function at Different Time Scales.** To investigate the possibility of a slow translational motion even in the samples with moderate humidities, i.e., without bulklike or confined water, we measured several samples with two different experimental resolutions, 93 and 35 $\mu$eV, respectively.

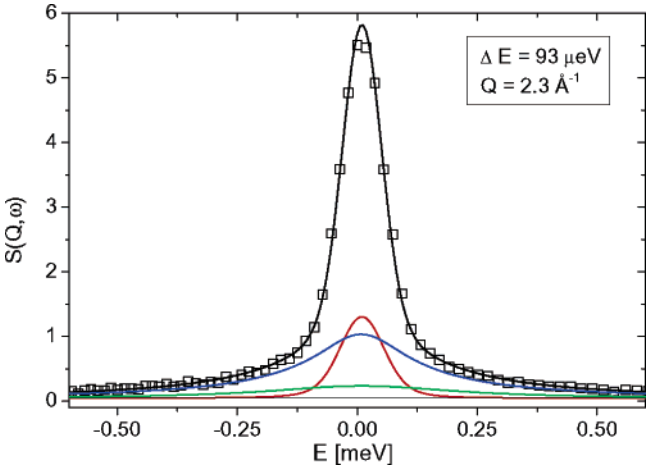


**Figure 4.** Example of experimental and fitted scattering function (double two-site jump model + excess water), sample at 100% r.h. and 296 K. The squares represent the experimental data and the connecting solid line shows the fitted scattering function. The single contributions stem from bulk water (blue line), the two two-site jump motions (red and green line), and a phenomenological background (thin black line).

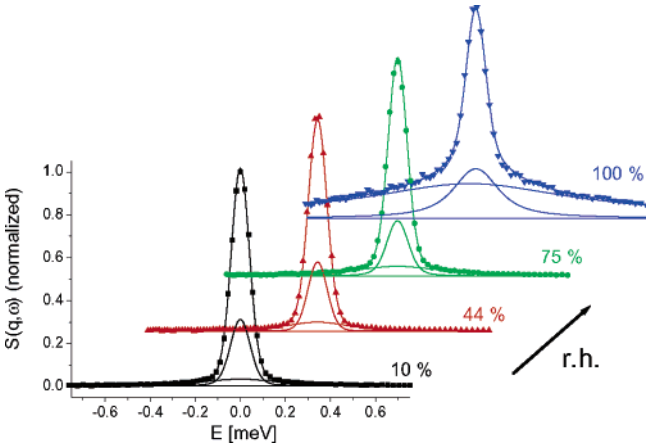


**Figure 5.** Scattering function of GO for increasing humidity at $Q = 2.3$ Å$^{-1}$: experimental data (solid symbols), fitted curves, and single quasielastic contributions (pseudo 3D presentation).

The data were fitted with the jump model described in the previous section. The fit for both resolutions yields rather identical results with the same fit parameters. The EISF and QISF values at the two different time scales overlap very well.

Thus, even at measurements with much smaller resolution function (35 $\mu$eV), no additional quasielastic contribution could be found, i.e., there is no indication for a possible slow translational motion in hydrated graphite oxide. This holds at least for time scales below ~30 ps. Therefore, the water in the interlayer space in graphite oxide at low and medium hydration levels can be regarded as being bound water, and the chosen double two-site jump model should be appropriate.

**3.6. Dependence on Humidity Level.** We investigated the motions in graphite oxide in dependence on the humidity level. Figure 5 shows an example of fitted data for four different humidity values.

It is clearly visible that the scattering contributions are very similar for the three lower humidity values (compare the lower three curves) but that they change distinctly for the highest humidity value (last curve). This indicates the same kind of underlying motions for lower humidities (10−75% r.h.) and the onset of a new type of motion for the last one (100% r.h.).

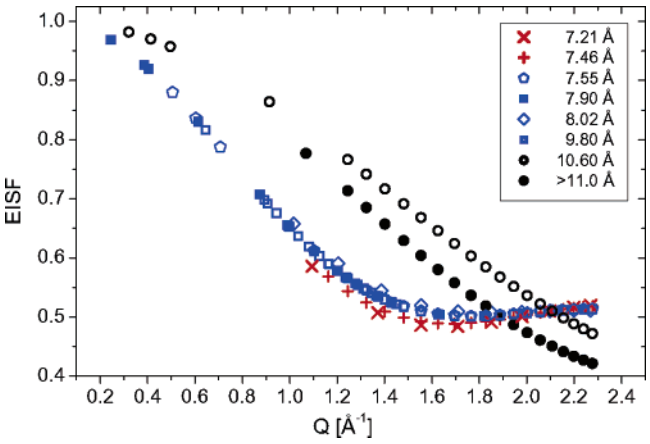


**Figure 6.** EISF for different humidity levels; the corresponding layer distances are given in the legend.

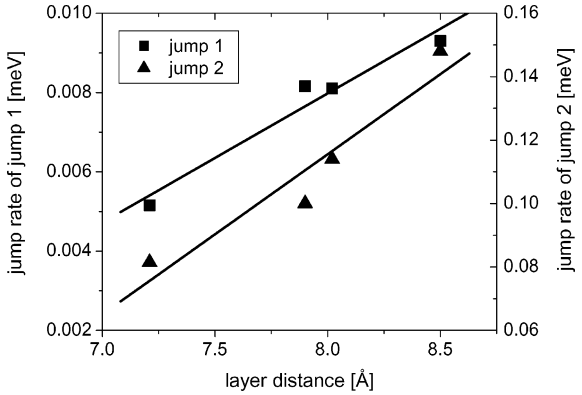


**Figure 7.** Layer-distance dependent jump rates of long (jump1) and short jumps (jump2).

In the next step, we investigate the behavior of the EISF, which demonstrates the changes of the quasielastic contributions and thus the changes of the occurring motions for increasing water content of the GO samples very distinctly.

The comparison of the behavior of EISF for different humidities and GO layer distances in Figure 6 shows explicitly that the kind of the hydration water does not change significantly except for the two highest hydration levels where excess water is present (highest layer distance: $d > 10.5$ Å, black circles). Very minor deviations are present for the almost dry samples with layer distances of 7.21 and 7.46 Å (red crosses).

For the following deeper analysis of the humidity-dependent behavior of GO, we divide the discussion of the results in two parts: samples with excess water (i.e., bulklike water or water with some constraints) and samples with bound water only (i.e., no excess water), as these two sample states behave completely different (see Figure 6). No intermediate state between these two cases has been detected. Graphite oxide samples contain excess water if the overall water content is high enough (in our case, 70 wt % absolute water content).

**Samples Without Excess Water, i.e., Layer Distance < 10 Å.** In the following, the behavior of jump rates, jump distances, and relative jump numbers will be analyzed in more detail.

The jump rates of both long and short jumps increase with increasing layer distance and water content (see Figure 7). Thus, one can conclude that the jump motions become less-hindered as more water is included.

For these samples without excess water, the relative number of the long jumps decreases with increasing layer distance and water content, whereas the relative number of short jumps

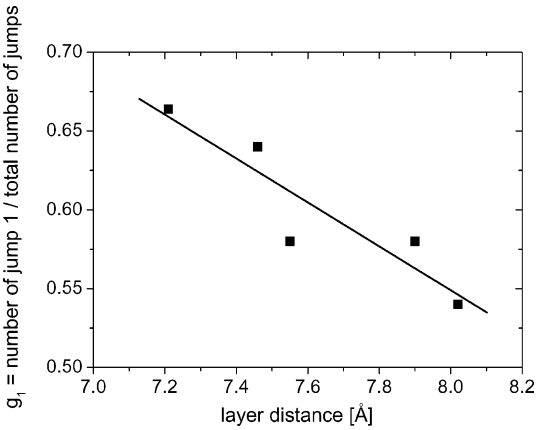


**Figure 8.** Layer-distance dependent ratio $g_1$ (number of jump1(long jumps)/total number of jumps).

increases with increasing layer distance and water content, see Figure 8.

In the next step we want to assign the fitted quasielastic contributions to certain motions in the hydrated graphite oxide.

*Assignment of Long Jumps.* As the number of water molecules in the interlayer space increases for higher humidity, the relative number of OH groups decreases. Therefore, we assume that "jump1" motions could come from motions of OH groups.

Nevertheless, the reduction of the relative number of jumps is not as big as would be expected from the amount of water taken up at each humidity step (theoretical values for composition $C_6O_3H_2$: 10 wt % absolute water content, 7.2 Å layer distance, 0.65 relative number of OH jumps; 14 wt % water, 7.5 Å, 0.56 OH jumps; 37 wt % water, 8.0 Å, 0.28 OH jumps; values were calculated from the relative amounts of GO and water for the given composition and humidity values but assuming all interlayer spaces are filled). Although the theoretical value agrees with the experimental one quite well for the almost dry sample (0.66 and 0.65), the mismatch increases with increasing water content. Thus one could possibly conclude that a part of the included water does not contribute to the jump motions, which would be another hint for the interstratification of empty interlayer spaces and fully or partly filled layers, see Section 3.2. Furthermore, the long jump motions could be increasingly less-hindered for higher humidities, thus increasing their fraction of jump number compared to the theoretical value at which all molecules and functional groups are expected to be in motion. Both possible reasons could justify the occurring discrepancy.

As the jump distances of both jump motions remain constant with increasing humidity level, we conclude that the OH jump motions take place between oxygen atoms (epoxide groups, OH groups) of one and the same layer, mainly by building and breaking hydrogen bonds. Otherwise, if the jumps would take place between oxygen atoms of adjacent layers, one would expect a change of jump distance with increasing layer spacing. Additionally, we can state that the hydrogen atom of the OH group can connect via hydrogen bonds with its facing layer or just by electrostatic interactions to neighboring oxygens of its own layer. These two possibilities are not distinguishable by means of neutron scattering, as the jump distance will be determined by only the distance of the oxygens the proton jumps between. However, one could assume that a coupling of the protons to the adjacent layer is much more probable compared with a coupling to the same layer, because cases in which a proton encounters suitable jump places in the nearest neighborhood of its own GO layer should be quite rare.

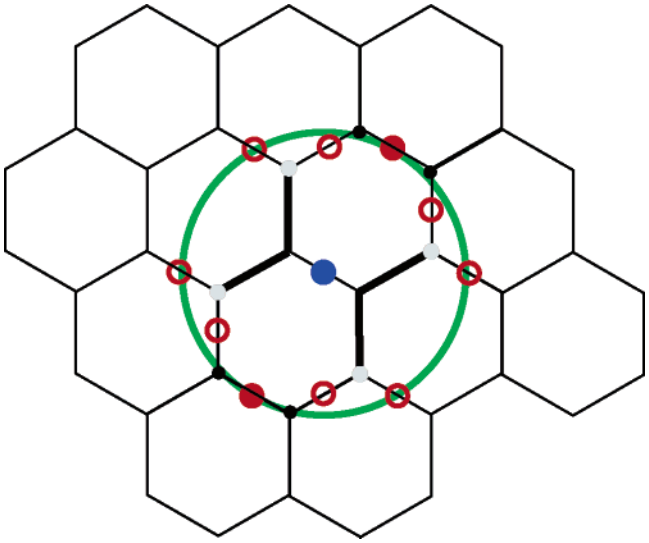

**Figure 9.** Stylized illustration of positions and distances within one GO layer. The carbon atoms are located in the corners of the hexagons. The (hollow and filled) red circles represent possible positions of epoxide groups and the gray and black dots show possible positions of OH groups. The blue circle in the middle marks the reference epoxide group.

Now, we want to justify and confirm the assignment of the long jumps to jumps of the protons of OH groups. To determine the possible positions and distances of the epoxide and OH groups, we consider the geometric illustration of the graphite oxide structure as given in Figure 9. Here, we follow only the possible jump positions and not the jumping proton. As the GO layers are mainly flat, it should be sufficient to regard only the two-dimensional structure. For this discussion, we also have to take into account on which side of the GO the functional groups are attached.

We start at an arbitrary position to place one epoxide group (blue circle in the middle) at the graphite oxide grid. It shall be situated above the carbon layer. The bonds next to our epoxide group (thick black lines) are not able to carry a second epoxide group, as the bonds are already saturated (as carbon is tetravalent).

In ref 38 it was stated that oxidized rings contain one epoxide and at least one OH group, and the C−OH and the epoxide groups are very close together, i.e., the OH groups could be placed at the very next positions (gray dots at the ends of the thick lines), whereas not all of the four positions necessarily have to be occupied by OH groups. At all four of these possible positions, the OH groups have to be placed below the carbon layer because of their van der Waals radii (otherwise they would be too close to the central epoxide group). The next possible positions for epoxide groups are marked with big red circles (filled and hollow), where the positions in direct neighborhood of the OH groups (gray dots) cannot be occupied when an OH group is present (hollow circles). If the possible positions of the epoxide groups are not filled, it is possible to place an OH group at the very next corner (small black dots). All of these groups can be situated above or below the carbon layer but according to steric conditions.

In Figure 9, it is clearly visible that all of these latter positions (i.e., besides the position of the central epoxide group) lie on or very close to a circle (green line) around the reference point. There are only the positions of the nearest OH groups (gray dots), which have a slightly smaller distance. But these are only 4 of 18 possible positions and thus do not contribute much to the found jump motion. Again, of course, not all of the possible positions carry epoxide or OH groups. Once an epoxide or OH group is placed, it rules out all of its neighboring positions according to steric and valence conditions.

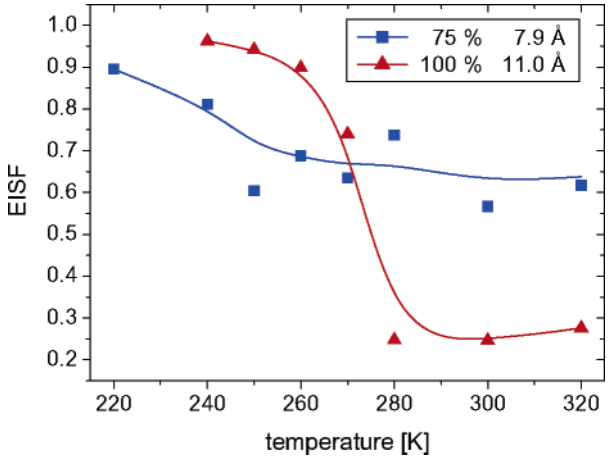


**Figure 10.** EISF vs temperature for 75 and 100% r.h. at $Q = 2.3$ Å$^{-1}$ (the lines are guides for the eye).

If we take about 1.5 Å as a typical C−C distance in the benzene rings, the radius of this circle can be calculated to about 3 Å which coincides very well with the jump distance determined for the long jumps.

This justifies the assignment of this long jump motion to jumps of the hydrogen atom of the OH groups between two positions of oxygen atoms (from epoxide or OH-groups) which should both belong to the next graphite oxide layer for most of the jumps.

The next possible positions for the epoxide and OH groups are not less than one C−C bond length outside of the marked circle. The necessary jump distance to these positions is at least 4 Å, which is for the proton not favorable to jump to, especially if there is an oxygen atom available at a shorter distance.

The chemical sum composition of the example area enclosed in the ring supports the earlier given distribution of epoxide and OH groups as well.

*Assignment of Short Jumps.* The jump distance of the short two-site jumps is 1.46 Å. The distance between the two hydrogen atoms of a water molecule is 1.5 Å. Thus, it agrees very well with the jump distance determined for the short jumps. Therefore, we assign the short jumps to 180° flips of isolated water molecules encapsulated in the interlayer space between the functional groups attached to the carbon grid.

From the previous investigations, it cannot be concluded whether the water molecules interact with the OH or the epoxide groups or both of them, but former NMR measurements suggest an interaction of the water protons with the OH groups rather than the epoxide groups.[24]

A quite comparable motion of water molecules was discussed in ref 39 for the monolayer hydrate of halloysite, which is a two-layer clay mineral. They described a 180 ° flip motion around the $C_2$-axis with the same jump distance, which also supports our assignment of this motion. The activation energy of the water flip motions in halloysite was higher ($E_A = 0.2$ eV) than in the GO sample with no excess water ($E_A = 0.075$ eV, see Figure 11). Consequently, the water molecules in graphite oxide are weaklier bound than in halloysite.

**Samples with Excess Water, i.e., Layer Distance > 10 Å.** The scattering function of the samples with high water content showed an additional broad contribution compared to the samples with lower humidities. These data could not be described by only the double two-site jump model used so far. As the

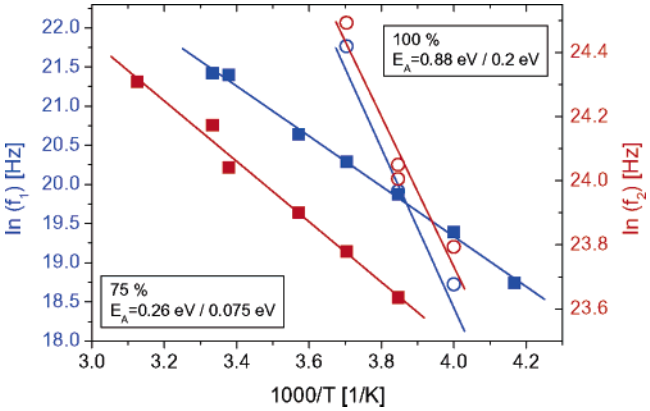


**Figure 11.** Arrhenius plot and resulting activation energies for jump1 and jump2 (solid squares, 75% r.h. sample; hollow circles, 100% r.h. sample; blue symbols, $f_1$; red symbols, $f_2$).

water content of these samples is remarkably higher, we supposed the presence of excess water. Bulklike or confined water can be situated in the interlayer space as well as in voids between the membrane patches.

We fitted this additional quasielastic contribution of the scattering function stemming from excess water with the Teixeira model[36] that takes into account a translational jump diffusion and classical rotational diffusion with the Sears expansion.[37] Thus, the fitted overall scattering function combined the Teixeira model and the double two-site jump model, with both contributions weighted according to the mass fractions.

As the contribution of the excess water was very dominating for these samples, the separation of the two two-site jumps appeared to be too ambiguous to draw similar conclusions about the behavior of jump rates and jump distances as in the previous paragraph. Consequently, in principle, only statements about the properties of the excess water are possible.

The diffusion constant of the translational diffusion of the excess water is in the range of the value for bulk water[40] ($D_{trans}$ = (2.0−2.3) × $10^{-9}$ $m^2/s$). The additional parameters for the description of the excess water are residence time $\tau_0 = 0.85$ ps and rotational diffusion coefficient $D_{rot} = 0.094$ meV.

As the side groups of GO (epoxide and OH groups) should be distributed on both sides of the graphite layer and on the basis of the found jump motions and the hydration behavior, as previously mentioned, it is reasonable to assume the successive filling of the interlayer space with water molecules. These water molecules couple via hydrogen bonds to certain jump places of both graphite surfaces. Hence, the interlayer space fills up continuously with up to two layers of (separated) water molecules. This process does not have to happen simultaneously for all interlayer spaces but successively with hydration level. The proposed interstratification effect also allows completely empty interlayer spaces. After the filling of one interlayer space with two water layers, additional water molecules will not be exceptional anymore compared to confined or even bulk water. The confinement itself can be caused by space restrictions.

For the samples with high humidity, the amount of water contained in the samples (up to 70 wt %) is too high to be distributed in the interlayer space only (maximum layer distance 11 Å). Moreover, as no intermediate sample state between samples with or without excess water was detected, one cannot distinguish between states where excess water is present in the interlayer space or in noninterlamellar voids between membrane patches.

**3.7. Dependence on Temperature.** The temperature behavior was investigated for two samples with 75 and 100% r.h. (corresponding to 34.9 and 70.0 wt % absolute water content, respectively), in the temperature range of 220−320 K.

Again, the behavior of the EISF reveals a qualitatively different behavior for both humidities, see Figure 10. The EISF for the 75% r.h. sample decreases only continuously with increasing temperature. Thus, it indicates a rise of quasielastic motions due to a higher mobility of water molecules and OH groups. In contrast, the EISF of the 100% r.h. sample drops suddenly at around 270 K. It demonstrates the melting of ice, which occurs only for the very humid samples. The water contained in the samples with moderate humidities does not undergo any freezing or melting process with temperature. This supports our previous assumption of widely separated water molecules in the graphite oxide, which interact mainly with the epoxide or OH groups rather than with other water molecules, thus preventing any freezing process.

Contrary to results from biological membranes,[41] we did not find any hysteresis effects of the layer distances and time constants with temperature, which could have been detected easily by following the Bragg peak positions. That means we do not face a process where the interlayer water is extracted from the interlayer space with decreasing temperature and reinserted with increasing temperature. In the biological membranes, the extracted water is stored in larger voids between the membrane stacks and therefore the crystallization to ice is possible. So in our case, all water stays between the graphite oxide layers during temperature scans.

The combination of this result with the nonfreezing of GO samples with moderate humidities also shows the sparse distribution of the water molecules, which prevents the formation of ice.

Furthermore, the investigation of the temperature dependence of the time constants $\tau$ will give information about the type of motions. The analysis of resulting activation energies leads to another alternative to assign the observed quasielastic contributions to certain motions.

As expected for noncooperative motions, both jump motions show an Arrhenius temperature behavior that can be described by

$$\tau = \tau_0 \exp\left(\frac{E_A}{kT}\right) \rightarrow \ln(f) = -\frac{E_A}{k}\frac{1}{T} + \text{constant} \qquad (6)$$

where $E_A$ is the activation energy, $\tau$ and $f = (1/2\pi\tau)$ are the relaxation time (i.e., mean residence time, see eq 4) and the relaxation frequency, respectively, the latter being illustrated in Figure 11.

The examination of the Arrhenius data results in the following activation energies $E_A$ for the two two-site jump motions: at 75% r.h., 0.26 eV for the long jumps and 0.075 eV for the short jumps; at 100% r.h., 0.88 and 0.2 eV, respectively.

The activation energies for the 100% r.h. sample are higher than those for the 75% r.h. sample. At first glance, this result seems to be in conflict with the increase in both jump rates with rising layer distance, as shown in Section 3.6. An increased layer distance could also have resulted in a lower activation energy. Thus, the uptake of additional water molecules accompanied by the higher layer spacings obviously leads to a stronger restriction of the motions observed under low- and medium-humidity conditions. This holds only for the 100% r.h. sample, as the water molecules are no longer widely separated and excess water is present, i.e., interactions between water molecules also influence the present motions.

With a more detailed evaluation of the two temperature-dependent parameters, MSD and jump ratio, for the 75% r.h.

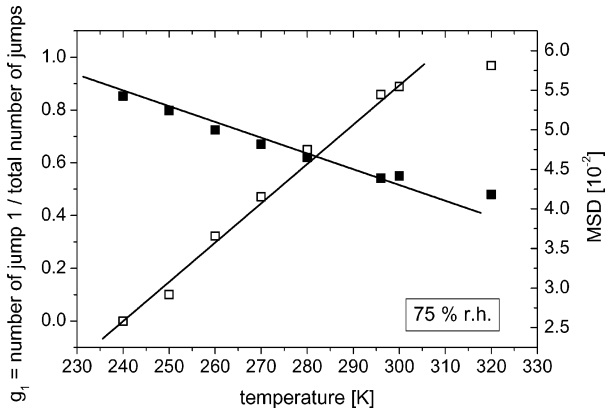


**Figure 12.** Ratio $g_1$ (jump1(long jumps)/total number of jumps) (solid symbols) and MSD (open symbols) for sample with 75% r.h.

sample, we can validate the types of motion even further. The mean square displacement MSD = $\langle u^2 \rangle$, which describes vibrational motions, increases linearly with increasing temperature, as displayed in Figure 12, i.e., no additional contribution shows up in the investigated temperature range.

The ratio of the number of jump1 motions (long jumps) to the total number of jumps decreases with increasing temperature, i.e., the relative number of long jumps decreases, thus indicating a proceeding rise of motions of the water molecules, as Figure 12 shows.

**3.8. Vibrational Density of States.** The evaluation of the vibrational density of states (DOS) allows some insight in the inelastic properties. We follow the well-known derivation as given in ref 42.

If we take into account only single-phonon processes, then

$$S(Q,\omega) = e^{-\langle u^2 \rangle Q^2}\{\delta(\omega) + \langle u^2 \rangle Q^2 S_1(\omega)\} \quad (7)$$

$$S_1(\omega) = [2\omega \sinh(\hbar\omega/2kT)]^{-1} e^{-\langle u^2 \rangle Q^2} g(\omega) \quad (8)$$

where $g(\omega)$ is the effective density of states and $e^{-\langle u^2 \rangle Q^2}$ is the Debye-Waller factor.

The density of states (see Figure 13, left) shows two main features, a rather small peak around 8 meV, which is correlated with intermolecular bending motions of water molecules, and a broad distinct peak around 60 meV, which is caused by librational modes of the water molecules.[43]

All observed vibrations should originate from water molecules included in the hydrated GO system. Intramolecular vibrations of OH groups typically have characteristic energies of more than 100 meV, which is outside of the accessible energy range of the current experiment. Additionally, both visible vibrational bands change depending on the hydration level, supporting the proposed origin.

As the peak indicating intermolecular motions of the water molecules is quite weak compared with those measured for bulk water or even confined water (see Figures 8 and 9 in ref 43), we conclude again the presence of only very rare intermolecular interactions between the water molecules. The bending peak is only more pronounced for the 100% r.h. sample.

This behavior proves now the assumption used for the evaluation of the fit model that in graphite oxide, the water molecules are sparsely distributed, and it rules out the relaxing cage model definitively. The water molecules present in the interlayer space of graphite oxide with low and moderate humidities cannot be described as confined water but only as bound water.

The comparison of the DOS for different humidity levels shows a small decrease in the intensity of the 8 meV bending mode with decreasing humidity, thus demonstrating the increasing hindrance of this intermolecular motion of the included water. This effect is in good agreement with findings for water in confined geometries.[44] In contrast to the results for confined water, we encounter a slight downshift of the 60 meV librational band for decreasing humidities, indicating weaker hydrogen bonds for samples with lower water content.[45] But, this result corresponds very well with the lower activation energies calculated for the samples with lower water content.

An indication for the presence of bulklike water in the 100% r.h. samples only is apparent in the representation of the data as dynamic susceptibility $S(\omega)/n(\omega)$ with the Bose factor $n(\omega) = [\exp(\hbar\omega/kT) - 1]^{-1}$, as given in Figure 13 (right). Thus, the discrimination between bulklike water and bound water is quite possible, because the α-resonance peak at around 0.4 meV is expected only for systems with bulklike water, as discussed in detail in ref 46.

We compare now the evaluation of the temperature-dependent DOS for the case with only interlayer water (75% r.h.) and the case where excess water is present (100% r.h.), see Figure 14.

This comparison of the behavior of the DOS for both samples reveals very distinct differences. For the lower-humidity sample, the height change in the bending peak (increase with decreasing temperature) is continuous and the peak shape does not alter. In contrast, the sample with higher humidity shows a different behavior and a clear freezing process can bee seen: There is a strong increase and change in shape of the 8 meV peak with decreasing temperature and also a large shift and shape change in the 60 meV peak (note the clear drop of the left slope). The

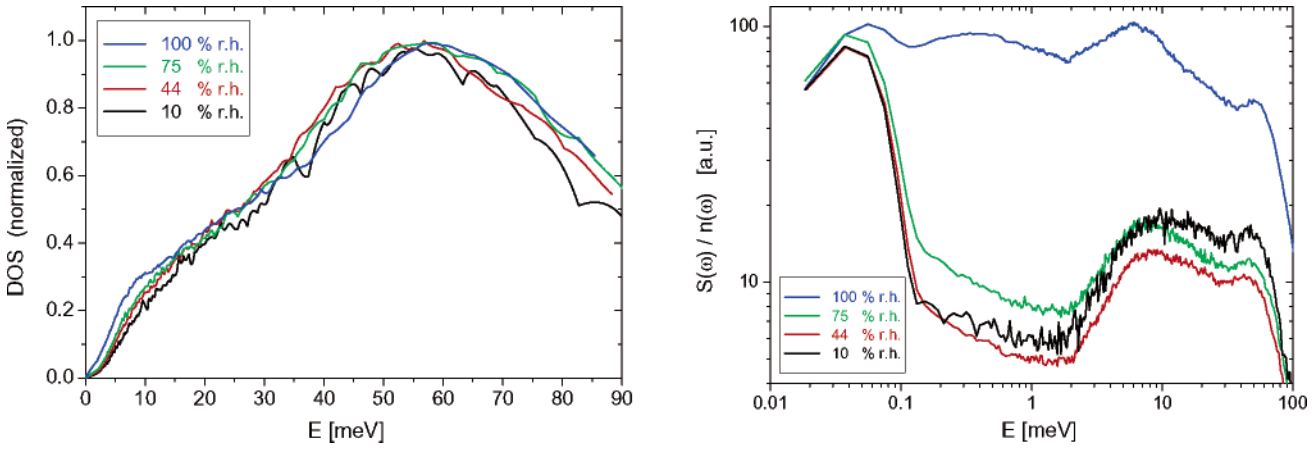


**Figure 13.** Humidity-dependent vibrational density of states (left) and dynamic susceptibility (right).

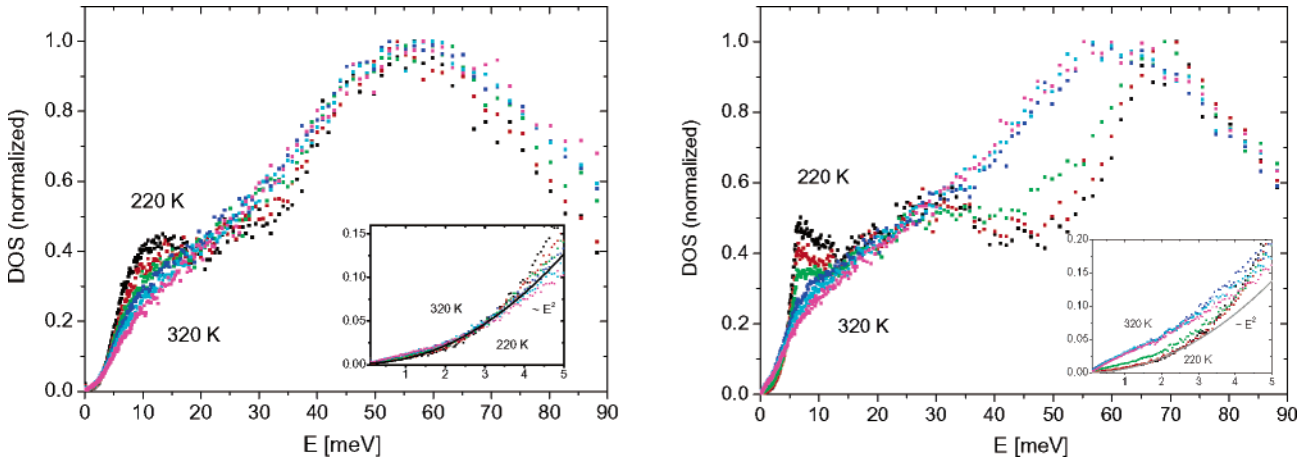


**Figure 14.** Vibrational density of states with 75% r.h. (left) and 100% r.h. (right) relative humidity, respectively. The insets show the enlarged range of low energy. For comparison reasons, an $E^2$ function is marked by a gray line.

sharp edge of the librational peak for the 100% r.h. sample clearly indicates the presence of crystalline hexagonal ice.[47]

As the bending peak decreases with increasing confinement (see the humidity-dependent behavior) the increase in the peak height with decreasing temperature marks a reduction of the water confinement for lower temperatures and a gradual adaptation to the behavior of confined water. This is especially apparent if one refers to the result for the high-humidity sample, where the formation of normal ice can also be concluded from the distinct change in the peak shape of the bending peak.

A more detailed analysis of the low-energy range, below 5 meV, shows again strong differences for both samples (see the insets of the figures). The 75% r.h. sample exhibits almost no temperature dependence in that energy range, and the energy dependence of the DOS follows the Debye type ($\sim E^2$) for all temperatures thus indicating that there is no change of the water type in the investigated temperature range. The 100% r.h. sample shows a clear temperature dependence, i.e., we get an additional contribution of vibrational states for temperatures above the freezing point (compare the deviations from the $E^2$ dependence), where the change of the curve is not a continuous one. The development of this contribution happens abruptly between 260 and 270 K.

This so-called "boson peak" is a typical feature for disordered, amorphous materials[48] and glassy systems, although not all disordered materials show this characteristic. Its origin is still debated in the literature. The temperature dependence of the boson peak can differ significantly for various materials, for instance, depending on their strong or fragile nature. In the 100% r.h. sample of graphite oxide, only the DOS for temperatures below the freezing point (below 270 K) follow the Debye behavior. This dependence is completely different from the behavior found for bound water like hydration shells in proteins, where the boson peak is present only for low temperatures and vanishes for temperatures above 180 K.[49,50] Consequently, the disappearance of the boson peak should, in our case, be related to the crystallization of bulklike or confined water during its freezing process. Thus, the different temperature-dependent DOS behavior proves the existence of liquid bulklike or confined water above the freezing point in only the 100% r.h. sample (boson peak above 270 K), but there are not these kinds of water within the 75% r.h. sample (no boson peak at any temperature).

A more detailed study of the density of states will follow in the future. Right now, we have discussed only the parts necessary for supporting our hypotheses about the nature of observed motions.

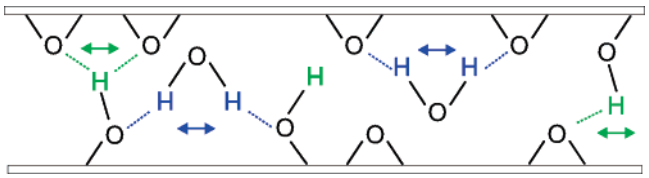

**Figure 15.** Model of dynamics in graphite oxide. The carbon grid is presented as flat layers for simplicity. The occurring motions of water molecules and OH groups are indicated with arrows. Possible hydrogen bonds are marked with dashed lines.

In summary, the investigated behavior of the humidity- and temperature-dependent vibrational density of states proves all the assumptions about the water included in the graphite oxide membrane stacks used so far: existence of excess (freezable) water only in samples with highest humidity, sparse distribution, and rare intermolecular interactions of water molecules; no humidity- and temperature-dependent change in water type for all other humidity levels.

## 4. Conclusions

We investigated the hydration behavior of layered graphite oxide as an inorganic model system with different hydration levels in the range of 10−100% relative environmental humidity.

The resulting layer distances were measured with X-ray scattering and quasielastic neutron scattering independently and ranged between 7 and 11 Å in our experiments.

The static structure of graphite oxide was revealed by former NMR investigations (existence and distribution of epoxide and OH groups).

With quasielastic neutron scattering, it could be shown that for samples without excess water, there exist only localized motions (on the investigated time scale, no long-range translational motion could be detected).

We assigned the two local motions to flipping motions of bound water molecules and OH groups. The data could be described by a double two-site jump model.

The kind of the existing water (bound water in interlamellar space) remained the same over almost the complete hydration range. Only the samples with highest water contents revealed the existence of bulklike or confined water (in the interlayer space as well as in noninterlamellar voids) which was demonstrated by the humidity- and temperature-dependent behavior of the elastic incoherent scattering factor (EISF) and the vibra-

tional density of states (DOS). The analysis of the humidity- and temperature-dependent density of states proved the sparse distribution of water molecules with only rare intermolecular interactions.

We did not face any stepwise filling of the membrane stacks with water. Instead of this, the hydration process starts with the filling of the intralamellar space and continues with the expansion of the interlamellar space but without any discontinuity.

It was not possible to distinguish between water molecules penetrating the GO layers (space between the functional groups) and water just in the interlamellar space, because the local environments of the water molecules are too similar (epoxide and OH groups in the nearest neighborhood). We also saw several indications for a random interstratification of empty interlayer spaces and fully (or partly) water filled layers, possibly caused by different oxidation levels of the single GO layers from the preparation process.

The discovered water-content-dependent properties of the graphite oxide bring us to the following model of the dynamics in GO (motions of water and OH groups) as displayed in Figure 15.

With the described hydration behavior, the graphite oxide shows some similarities with two-layer clay minerals as halloysite,[39] which have no charged surfaces, whereas the water dynamics in three-layer clay minerals is quite different.[51] The similarities and differences arise mainly from the property of charged surfaces. Two-layer clay minerals and graphite oxide have no charges at the layer surfaces, whereas three-layer clay minerals possess charged surfaces.

In conclusion, the hydration behavior is mainly determined by the synthesis method (number and distribution of epoxide and OH groups), the hydration process (amount of sample, equilibration time, amount and distribution of water molecules), and the surface charge of the membrane layers. The water molecules in the interlayer space are bound via hydrogen bonds to oxygen atoms of epoxide and OH groups undergoing only localized motions, which can be described by a double two-site jump model.

**Acknowledgment.** The authors thank H. P. Boehm (Ludwig-Maximilians-Universität, München) and I. Dekany and T. Szabo (University of Szeged) for providing the graphite oxide samples and the BENSC technical staff of HMI Berlin for the help during preparation of the experiments.

## References and Notes

(1) Brodie, B. C. *Ann. Chim. Phys.* **1860**, *59*, 466.
(2) Yazami R.; Touzain, Ph. *Synth. Met.* **1985**, *12*, 499.
(3) Mermoux, M.; Yazami, R.; Touzain, Ph. *J. Power Sources* **1987**, *20*, 105.
(4) Cassagneau, T.; Fendler, J. H. *Adv. Mater.* **1998**, *10*, 877.
(5) Hwa, T.; Kokufuta, E.; Tanaka, T. *Phys. Rev. A* **1991**, *44*, R2235.
(6) Wen, X.; Garland, C. W.; Hwa, T.; Kardar, M.; Kokufuta, E.; Li, Y.; Orkisz, M.; Tanaka, T. *Nature (London)* **1992**, *355*, 426.
(7) Abraham, F. F.; Goulian, M. *Europhys. Lett.* **1992**, *19*, 293.
(8) Kotov, N. A.; Dekany, I.; Fendler, J. H. *Adv. Mater.* **1996**, *8*, 637.
(9) Kovtyukhova, N. I.; Ollivier, P. J.; Martin, B. R.; Mallouk, T. E.; Chizhik, A.; Buzaneva, E. V.; Gorchinskiy, A. D. *Chem. Mater.* **1999**, *11*, 771.
(10) Brodie, B. C. *Liebigs Ann. Chem.* **1860**, *114*, 6.
(11) Thiele, H. *Z. Anorg. Allg. Chem.* **1930**, *190*, 145.
(12) Hofmann, U.; Frenzel, A.; Csalan, E. *Liebigs Ann. Chem.* **1934**, *510*, 1.
(13) Hofmann, U.; Holst, R. *Ber. Dtsch. Chem. Ges.* **1939**, *72*, 754.
(14) Ruess, G. *Kolloid Z.* **1945**, *110*, 17.
(15) DeBoer, J. H.; van Doorn, A. B. C. *Proc. K. Ned. Akad. Wet., Ser. B* **1954**, *57*, 181.
(16) Clauss, A.; Plass, R.; Boehm, H.-P.; Hofmann, U. *Z. Anorg. Allg. Chem.* **1957**, *291*, 205.
(17) Scholz, W.; Boehm, H.-P. *Z. Anorg. Allg. Chem.* **1969**, *369*, 327.
(18) Boehm, H.-P.; Scholz, W. *Liebigs Ann. Chem.* **1966**, *691*, 1
(19) Staudenmaier, L. *Ber. Dtsch. Chem. Ges.* **1899**, *31*, 1481.
(20) Ruess, G. *Monatsh. Chem.* **1946**, **76**, 381.
(21) Nakajima, T.; Mabuchi, A.; Hagiwara, R. *Carbon* **1988**, **26**, 357.
(22) Mermoux, M.; Chabre, Y. *Synth. Met.* **1989**, *34*, 157.
(23) Mermoux, M.; Chabre, Y.; Rousseau, A. *Carbon* **1991**, *29*, 469.
(24) Lerf, A.; He, H.; Forster, M.; Klinowski, J. *J. Phys. Chem. B* **1998**, *102*, 4477.
(25) Lerf, A.; He, H.; Riedl, T.; Forster, M.; Klinowski, J. *Solid State Ionics* **1997**, *101*−*103*, 857.
(26) Titelman, G. I.; Gelman, V.; Bron, S.; Khalfin, R. L.; Cohen, Y.; Bianco-Peled, H. *Carbon* **2005**, *43*, 641.
(27) DeBoer, J. H.; van Doorn, A. B. C. *Proc. K. Ned. Akad. Wet., Ser. B* **1958**, *61*, 242.
(28) Lerf, A.; Buchsteiner, A.; Pieper, J.; Schöttl, S.; Dekany, I.; Szabo T.; Boehm, H.-P. *J. Phys. Chem. Solids* **2006**, *67*, 1106.
(29) Hummers, W. S.; Offeman, R. E. *J. Am. Chem. Soc.* **1958**, *80*, 1339.
(30) Schmitt, H.-J. Diploma thesis; University of Heidelberg, Heidelberg, Germany, 1969.
(31) Rufflé, B.; Ollivier, J.; Longeville, S.; Lechner, R. E. *Nucl. Instrum. Methods Phys. Res., Sect. A* **2000**, *449*, 322.
(32) Rufflé, B. *Fitmo User Manual*; Hahn-Meitner-Institut: Berlin, 2000.
(33) Van Hove, L. *Phys. Rev.* **1954**, *95*, 249.
(34) Bée, M. *Quasielastic Neutron Scattering*; Adam Hilger: Philadelphia, PA, 1988.
(35) Chen, S.-H.; Liao, C.; Sciortino, F.; Gallo, P.; Tartaglia, P. *Phys. Rev. E* **1999**, *59*, 6708.
(36) Teixeira, J.; Bellissent-Funel, M.-C.; Chen, S. H.; Dianoux, A. J. *Phys. Rev. A* **1985**, *31*, 1913.
(37) Sears, V. F. *Can. J. Phys.* **1966**, *44*, 1279; *45*, 237.
(38) He, H.; Klinowski, J.; Forster, M.; Lerf, A. *Chem. Phys. Lett.* **1998**, *287*, 53.
(39) Cruz, M. I.; Letellier, M.; Fripiat, J. J. *J. Chem. Phys.* **1978**, *69*, 2018.
(40) Bellissent-Funel, M.-C. *J. Mol. Liq.* **2000**, *84*, 39.
(41) Fitter, J.; Lechner, R. E.; Dencher, N. A. *J. Phys. Chem. B* **1999**, *103*, 8036.
(42) Lechner, R. E.; Richter, D.; Riekel, C. *Springer Tracts in Modern Physics 101*; Springer-Verlag: New York, 1983.
(43) Crupi, V.; Majolino, D.; Migliardo, P.; Venuti, V. *J. Phys. Chem. B* **2002**, *106*, 10884.
(44) Crupi, V.; Dianoux, A. J.; Majolino, D.; Migliardo P.; Venuti, V. *Phys. Chem. Chem. Phys.* **2002**, *4*, 2768.
(45) Venables, D. S.; Huang, K.; Schmuttenmaer, Ch. A. *J. Phys. Chem. B* **2001**, *105*, 9132.
(46) Settles, M.; Doster, W. *Faraday Discuss.* **1996**, *103*, 269.
(47) Kolesnikov, A. I.; Zanotti, J.-M.; Loong, C.-K.; Thiyagarajan, P.; Moravsky, A. P.; Loutfy, R. O.; Burnham, C. J. *Phys. Rev. Lett.* **2004**, *93*, 035503−1.
(48) Rachwalska, M.; Natkaniec, I. *Physica B* **2004**, *348*, 371.
(49) Paciaroni, A.; Bizzarri, A. R.; Cannistraro, S. *Phys. Rev. E* **1998**, *57*, R6277.
(50) Paciaroni, A.; Bizzarri, A. R.; Cannistraro, S. *Phys. Rev. E* **1999**, *60*, R2476.
(51) Swenson, J.; Bergman, R.; Howells, W. S. *J. Chem. Phys.* **2000**, *113*, 2873.